JOURNAL OF SPACECRAFT AND ROCKETS
Vol. 32, No. 2, March–April 1995

Mars Pathfinder Trajectory Based Heating and Ablation Calculations

Y.-K. Chen,* W. D. Henline,† and M. E. Tauber‡
NASA Ames Research Center, Moffett Field, California 94035-1000

The Mars Pathfinder probe will enter the Martian atmosphere at a relative velocity of 7.65 km/s. The 2.65-m-diam vehicle has a blunted, 70-deg-half-angle, conical forebody aerobrake. Axisymmetric time-dependent calculations have been made using Gauss–Seidel implicit aerothermodynamic Navier–Stokes code with thermochemical surface conditions and a program to calculate the charring-material thermal response and ablation for heating analysis and heat-shield material sizing. The two codes are loosely coupled. The flowfield and convective heat-transfer coefficients are computed using the flowfield code with species balance conditions for an ablating surface. The time-dependent in-depth conduction with surface blowing is simulated using the material response code with complete surface energy-balance conditions. This is the first study demonstrating that the computational fluid-dynamics code interfacing with the material response code can be directly applied to the design of thermal protection systems of spacecraft. The heat-shield material is SLA-561V. The solutions, including the flowfield, surface heat fluxes and temperature distributions, pyrolysis-gas blowing rates, in-depth temperature history, and minimum heat-shield thicknesses over the aeroshell forebody, are presented and discussed in detail. The predicted heat-shield mass is about 20 kg.

Nomenclature

B = pre-exponential factor, Eq. (4), s^{-1}
B' = dimensionless mass-loss rate
C_H = heat-transfer Stanton number
C_M = mass-transfer Stanton number
D = diffusion coefficient, m^2/s
E_a = activation energy, Eq. (4), K
F = radiation view factor
h = enthalpy, J/kg
h_c = enthalpy of char, J/kg
h_{ew} = wall enthalpy, defined in Ref. 6, J/kg
h_g = enthalpy of pyrolysis gas, J/kg
h_r = recovery enthalpy, J/kg
$\dot{m}_c$ = char mass flow rate, $kg/m^2 \cdot s$
$\dot{m}_g$ = pyrolysis-gas mass flow rate, $kg/m^2 \cdot s$
N_r = total number of surface reactions
N_s = total number of species
q_{cond} = in-depth conductive heat flux, W/m^2
q_{rad} = radiative heat flux, W/m^2
R_b = base radius, m
R_c = corner radius, m
R_n = nose radius, m
S = distance along surface from stagnation point, m
T = temperature, K
t = time from 125-km altitude, s
u_e = velocity at edge of boundary layer, m/s
v = velocity component normal to surface, m/s
x = mass fraction
Z^* = weighted average of the mole and mass fractions, defined in Ref. 6
α = surface absorption coefficient
ε = surface emissivity
η = coordinate normal to surface, m
θ = time, s
ρ = density, kg/m^3
ρ_e = density at edge of boundary layer, kg/m^3
ρ_o = original density of ablator, Eq. (4), kg/m^3
ρ_r = residual density of ablator, Eq. (4), kg/m^3
σ = Stefan–Boltzmann constant, $W/m^2 \cdot K^4$
Ψ = decomposition reaction order, Eq. (4)
ω = mass flux of chemical reactions, $kg/m^2 \cdot s$

Received Aug. 16, 1994; revision received Nov. 1, 1994; accepted for publication Nov. 28, 1994.

*Research Scientist, Thermosciences Institute, MS 234-1.
†Research Scientist, Reacting Flow Environment Branch, MS 230-2.
‡Research Scientist, Reacting Flow Environment Branch, MS 229-3. Associate Fellow AIAA.

Introduction

PREVIOUS proposals have been made for a Mars Environment Survey (MESUR) mission to land a globally distributed set of 16 small, well-instrumented packages on Mars to make observations of the atmosphere and the planetary surface.[1] A precursor probe–lander to the MESUR mission is the Mars Pathfinder. The probe will enter the Martian atmosphere at a relative velocity of 7.65 km/s. The forebody is a blunted, 70-deg-half-angle cone, based on the Viking Mars lander shape.[2] The forebody diameter is 2.65 m, and a ballistic coefficient of 55 kg/m^2 is used. The Mars Pathfinder probe will experience heating rates and deceleration loads that are nearly an order of magnitude greater than those encountered by the Viking vehicles.[2] Therefore, the design of the aerobrake is a more difficult task. Previous viscous-shock-layer[3] and Navier–Stokes calculations[4] for flow over a nonablating aeroshell provided information for a preliminary design study for aerobrakes for MESUR.[5] Based on that preliminary study, the heat-shield material used on Viking (a silicone elastomeric charring ablator, SLA-561V) was again selected as the tentative candidate material for the Mars Pathfinder aeroshell heat shield. The objective of this study is to determine the heat-shield thickness distribution and mass that yields the maximum total heat load for what is currently the trajectory with the shallowest entry angle (−14.3 deg at 125 km).

The accurate prediction of the aerothermal heating over a charring ablator requires a time-dependent calculation through the entire trajectory. This is necessary because pyrolysis gas-blowing rates depend on the ablator-material in-depth temperature history. The program CMA[6] was designed to simulate the thermal response of charring ablators. In CMA, the heat flux to the ablating surface is usually computed based on the input nonablating heat-transfer coefficients and empirical blowing-reduction parameters. The uncertainty in this estimated ablating surface heat flux is high, and consequently the predictions of surface blowing rate and temperature are somewhat inaccurate. Thus, in order to obtain the best

estimated heat flux over an ablating surface, a flow solver with ablating surface conditions becomes a requirement. The flowfield over the Mars Pathfinder aeroshell cannot be precisely resolved without using full Navier–Stokes equations, because of the large subsonic region in its shock layer. Since the surface blowing rate is expected to be moderate, the approach taken in this study is to combine solutions from the GIANTS[7] (Gauss–Seidel implicit aerothermodynamic Navier–Stokes code with thermochemical surface conditions) and CMA codes in a loosely coupled manner, such that both the flow solver (GIANTS) and the thermal response code (CMA) can share the correct ablating surface conditions without major code modification. The computations using GIANTS with complete ablating surface species balance conditions are performed at a certain number of selected trajectory points utilizing the surface blowing rate and the temperature profiles obtained from CMA. The time-dependent computations of CMA with complete surface energy-balance conditions are performed over the entire forebody heat shield using the convective heat-transfer coefficients calculated from GIANTS.

Computational Methods

The GIANTS code is a two-dimensional axisymmetric nonequilibrium full Navier–Stokes equation solver that has been modified to include the ablating surface species balance condition:[8]

$$\rho D_i \frac{\partial x_i}{\partial \eta}\bigg|_w + \dot{m}_g x_{gi} + \dot{m}_c x_{ci} = \rho v x_i + \sum_{r=1}^{N_r} \omega_i^r \qquad (i = 1, \ldots, N_s) \tag{1}$$

The velocity component normal to the surface (v) is obtained from

$$v = (\dot{m}_g + \dot{m}_c)/\rho \tag{2}$$

For each global iteration, the GIANTS calculations are performed with fixed temperature and mass-blowing rate distributions over the surface. These input values are updated iteratively from the CMA calculations.

The CMA code is used for the transient thermal and ablation response of a charring insulation material structure, utilizing a complete surface energy-balance condition:

$$\rho_e u_e C_H (h_r - h_{ew}) + \rho_e u_e C_M \left(\sum_i (Z_{ie}^* - Z_{iw}^*) h_i^{Tw} - B' h_w \right)$$

$$+ \dot{m}_c h_c + \dot{m}_g h_g + \alpha_w q_{\text{rad}} - F\sigma\varepsilon_w T_w^4 - q_{\text{cond}} = 0. \tag{3}$$

This surface energy balance includes ablation, radiation, and in-depth conduction. (An extensive discussion of the energy-balance equation is presented in the CMA user's manual.[6]) The CMA code obtains the convective heat-transfer coefficients from GIANTS solutions, plus the net radiative heat fluxes to the surface using correlations[9] at various times and locations.

To properly represent the heating trend along the entire trajectory, 21 points are selected from the trajectory (Fig. 1), in which the convective heat-transfer coefficients are computed by the GIANTS code. The points are selected according to their estimated stagnation-point heating so that the difference in heating between two neighboring points is approximately the same. The flight and freestream conditions at the selected trajectory points are listed in Table 1. For each global iteration, the steady-state GIANTS solutions are obtained for all points except the first three, where the freestream densities are very low. Previous experience showed that the computational domain has to be extended into part of the afterbody region, and the total number of iterations required is substantially increased to obtain a converged flow solution when the freestream density is very low. Consequently, the computation can become excessively expensive. Moreover, the accuracy of Navier–Stokes solutions for very low-density flows is degraded. Thus, instead of solving the very expensive Navier–Stokesequations, the heat fluxes for the first three points are estimated using an extrapolation method. The convective heat fluxes for the first three points are very low compared with the rest of points; therefore, some uncertainty in heat fluxes for these three points will not create significant error in the analysis.

Table 1 Trajectory points selected for GIANTS calculations

Time, s	V, m/s	Altitude, m	T, K	Density, kg/m^3
14	7661.1	99,930	139.0	0.138E − 6
24	7665.7	83,516	139.0	0.137E − 5
30	7661.0	74,280	139.1	0.497E − 5
34	7647.3	68,386	140.1	0.113E − 4
37	7624.5	64,110	142.0	0.206E − 4
40	7582.5	59,967	144.2	0.359E − 4
42	7540.1	57,284	146.4	0.488E − 4
45	7447.7	53,386	149.5	0.761E − 4
47	7361.1	50,880	152.0	0.101E − 3
50	7181.9	47,272	155.0	0.153E − 3
56[a]	6592.3	40,696	162.0	0.324E − 3
60	6007.4	36,866	166.5	0.501E − 3
62	5667.2	35,135	168.7	0.600E − 3
64	5312.1	33,530	171.0	0.703E − 3
66	4950.9	32,046	172.5	0.813E − 3
68	4591.7	30,680	175.0	0.931E − 3
70	4241.6	29,426	176.0	0.105E − 2
73	3745.7	27,735	177.4	0.124E − 2
76	3295.4	26,249	180.0	0.144E − 2
81	2658.5	24,149	183.0	0.177E − 2
90	1837.0	21,229	186.8	0.236E − 2

[a]Peak convective heating point.

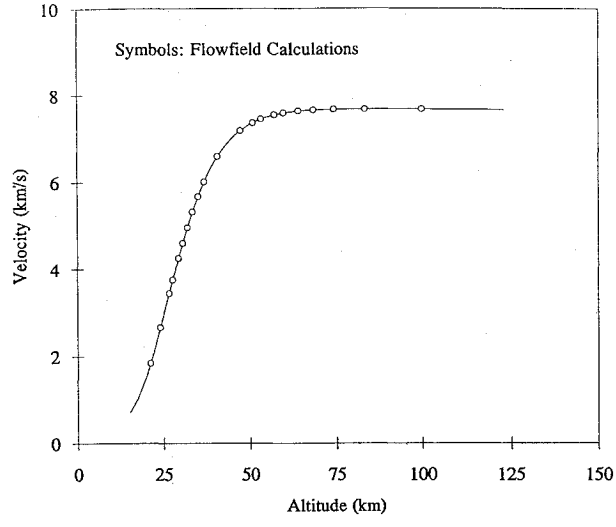

Fig. 1 Trajectory for MESUR pathfinder.

The structure of CMA is one-dimensional. Hence, for each computational cell at the surface, in-depth conduction into the ablation material is assumed to be one-dimensional. In this study, 40 computational cells are used along the forebody surface. Therefore, the CMA code has to be run 40 times independently in each global iteration to obtain the surface blowing rate and temperature distributions over the entire forebody along the entry trajectory.

Because the surface blowing rate is expected to be low, a loosely coupled method is adopted here. In the first global iteration for a given trajectory point, the nonequilibrium calculations start from the GIANTS code with nonablating surface conditions, and then the resulting heat-transfer coefficients for this trajectory point are used in CMA. The CMA code integrates from $t = 0$ to this trajectory point to obtain simulations of the transient thermal and ablation response over the entire forebody. The new surface temperature and blowing-rate distributions obtained from CMA are supplied to GIANTS to start a new global iteration. The computation for this trajectory point is completed and advanced to next trajectory point when the variations of surface temperature and blowing rates are less than 0.1%.

Chemistry Model

Fourteen gas species (CO_2, CO, N_2, O_2, NO, SiO, H_2, C_2, C_3, C, N, O, H, and Si) and 19 gas chemical reactions are used. The chemical reactions include

$$CO_2 + M1 \rightleftharpoons CO + O + M1 \quad \text{(R1)}$$

$$CO + M2 \rightleftharpoons C + O + M2 \quad \text{(R2)}$$

$$N_2 + M3 \rightleftharpoons N + N + M3 \quad \text{(R3)}$$

$$O_2 + M4 \rightleftharpoons O + O + M4 \quad \text{(R4)}$$

$$NO + M5 \rightleftharpoons N + O + M5 \quad \text{(R5)}$$

$$C_2 + M6 \rightleftharpoons C + C + M6 \quad \text{(R6)}$$

$$C_3 + M7 \rightleftharpoons C + C_2 + M7 \quad \text{(R7)}$$

$$H_2 + M8 \rightleftharpoons H + H + M8 \quad \text{(R8)}$$

$$SiO + M9 \rightleftharpoons Si + O + M9 \quad \text{(R9)}$$

$$CO + N \rightleftharpoons NO + C \quad \text{(R10)}$$

$$CO + CO \rightleftharpoons CO_2 + C \quad \text{(R11)}$$

$$CO + O \rightleftharpoons O_2 + C \quad \text{(R12)}$$

$$N_2 + O \rightleftharpoons NO + N \quad \text{(R13)}$$

$$NO + CO \rightleftharpoons CO_2 + N \quad \text{(R14)}$$

$$NO + O \rightleftharpoons O_2 + N \quad \text{(R15)}$$

$$CO_2 + O \rightleftharpoons O_2 + CO \quad \text{(R16)}$$

$$Si + NO \rightleftharpoons SiO + N \quad \text{(R17)}$$

$$Si + CO_2 \rightleftharpoons SiO + CO \quad \text{(R18)}$$

$$Si + O_2 \rightleftharpoons SiO + O \quad \text{(R19)}$$

The rate coefficients of the reactions are from Refs. 10–12. The surface temperature over the Mars Pathfinder aeroshell is not high enough to generate a significant amount of char sublimation. Therefore, the blowing rate of the pyrolysis gas becomes the major focus of the present calculation. To perform the simulation, CMA was modified according to the following assumptions: 1) the pyrolysis gas itself is in chemical equilibrium with the char before it interacts with the mainstream species, and consists of 4 elements[13] (H, C, O, and Si) and 11 species (CO_2, CO, O_2, SiO, H_2, C_2, C_3, C, O, H, and Si); 2) the char blowing rate is set to zero; 3) the first-order fully catalytic CO + O recombination reaction is the only dominant surface reaction used in the source term (last term) of Eq. (1); 4) the surface enthalpy is calculated from the local temperature, pressure, and the species concentrations obtained from Eq. (1); and 5) the decomposition of SLA-561V into char and pyrolysis gas follows the relation[13]

$$\left.\frac{\partial \rho}{\partial \theta}\right|_{\eta} = -B \exp\left(\frac{-E_a}{T}\right) \rho_o \left(\frac{\rho - \rho_r}{\rho_o}\right)^{\Psi} \quad (4)$$

where $B = 2.78 \times 10^{10}\ s^{-1}$, $E_a = 19{,}000$ K (34,200 R), and $\Psi = 3$.

Results and Discussion

The computations are performed using the NASA NAS (numerical aerodynamics simulation program) Cray C90 supercomputer. The forebody of Mars Pathfinder is a spherically blunted cone with a 70-deg half angle, $R_n = 0.6625$ m, $R_b = 1.325$ m, and $R_c = 0.06625$ m. A 42 × 82 computational grid is used in the GIANTS code, and a 32-node nonuniform grid in the CMA calculations for each surface station. The grid sensitivity study for GIANTS has been performed to ensure that the grids were adequate for the current study, and the solutions at the peak heating point were

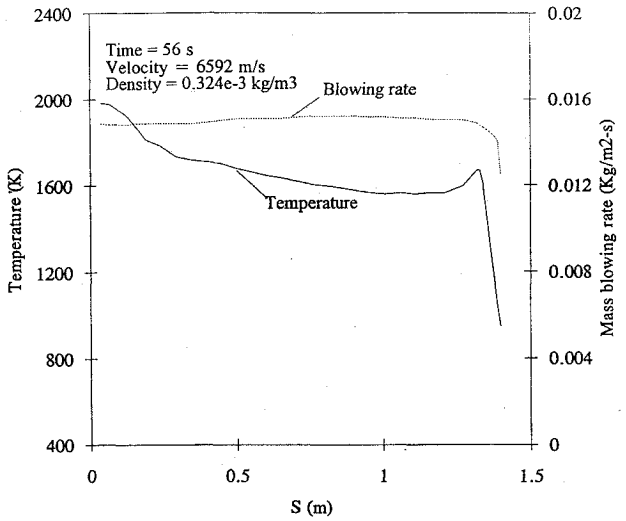

Fig. 2a Temperature and blowing rate distributions.

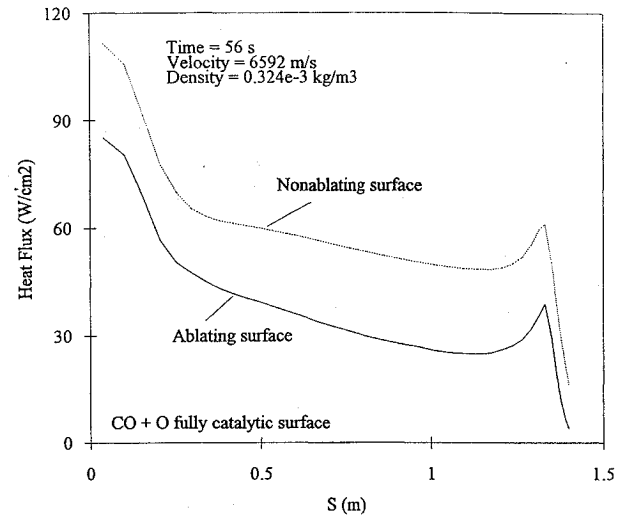

Fig. 2b Convective heat-flux distribution.

compared with those of the LAURA code.[14] In view of the peculiarities of the explicit scheme used in CMA, the time steps used in the calculation were very carefully controlled for the best possible solutions. The solutions presented here are for a maximum variation of surface temperature and blowing rates of less than 0.1%. Surface temperature, heat flux, and blowing rates as functions of time and location will be shown in the following section. Comparison of heat fluxes between the ablating and nonablating surface conditions is also included. Also, in-depth temperature histories for SLA-561V at various locations along forebody are presented, followed by detailed flowfields over the aeroshell forebody. Finally, the resultant heat-shield thicknesses are shown as a function of body station.

The surface temperature (solid line) and mass-blowing-rate (dotted line) distributions along the aeroshell forebody at the peak convective heating point ($t = 56$ s) are shown in Fig. 2a. The temperature at the stagnation point is near 2000 K, and it drops to below 1600 K along the conical forebody region. The mass blowing rate of the pyrolysis gas remains fairly uniform in both the spherical and conical regions, and is about 0.7% of the freestream mass flow rate at peak heating. The mass-blowing-rate and temperature distributions do not appear to be very smooth along the body surface. This is the result of the explicit scheme adopted in CMA and the assumption of the one-dimensional in-depth conduction model applied in the computation. The surface heat-flux distributions for both ablating and nonablating conditions at the peak heating point are presented in Fig. 2b. Since, for conservatism, the surface is assumed to be fully catalytic for the CO + O recombination reaction, the predicted heating is very sensitive to the transport properties, especially for the nonablating surface condition. The transport properties adopted here are the same as

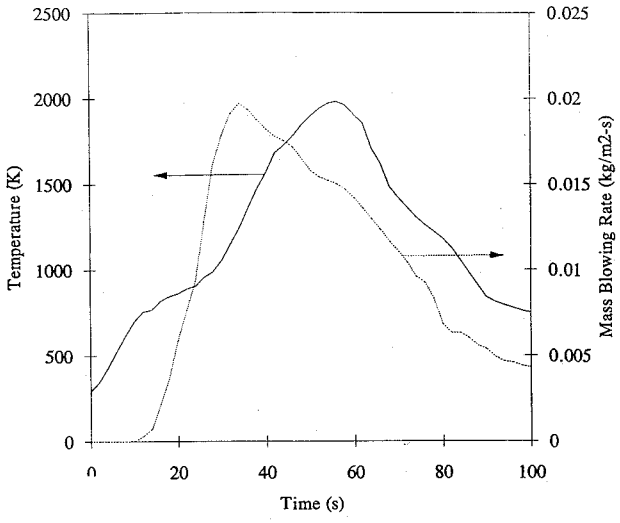

Fig. 3a Stagnation-point temperature and mass-blowing-rate history.

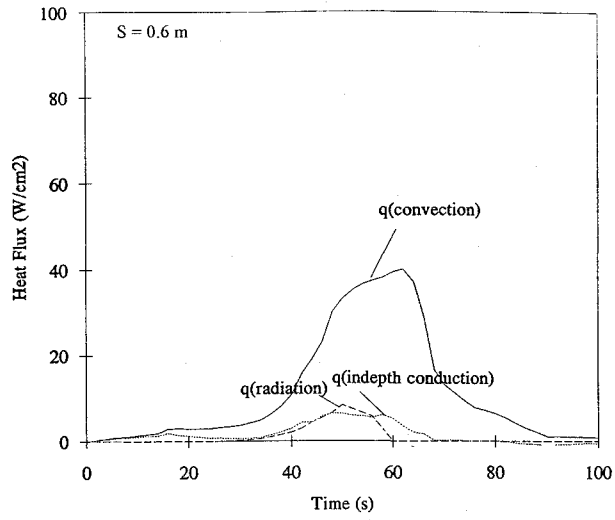

Fig. 4b Surface heat-flux history.

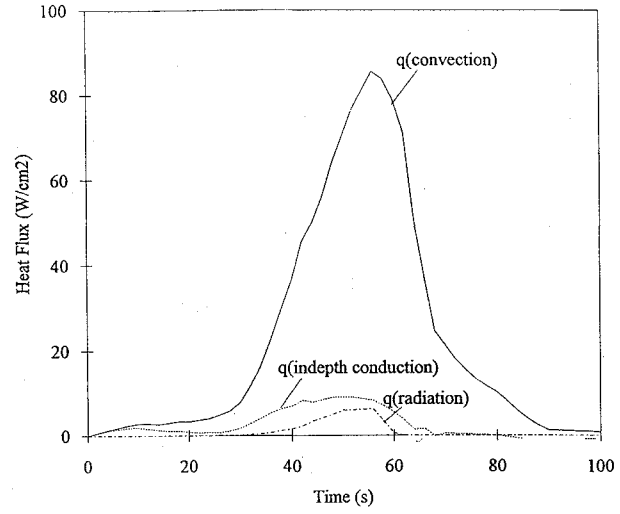

Fig. 3b Stagnation-point surface heat-flux history.

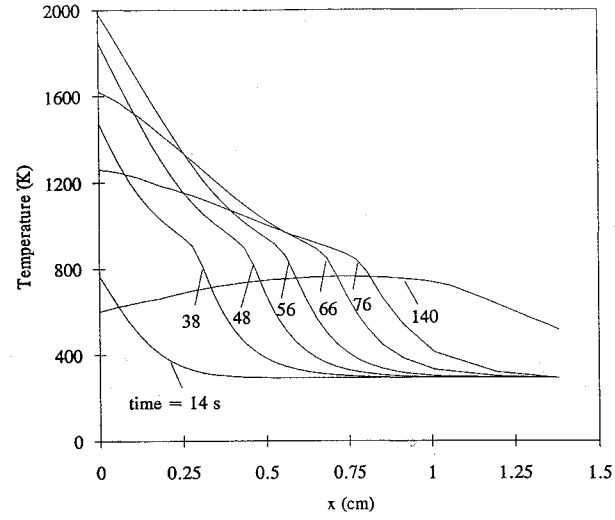

Fig. 5a Stagnation-point in-depth temperature history.

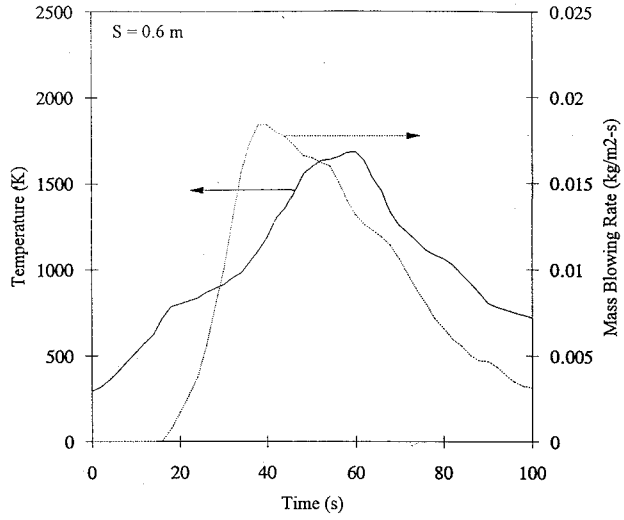

Fig. 4a Temperature and mass-blowing-rate history.

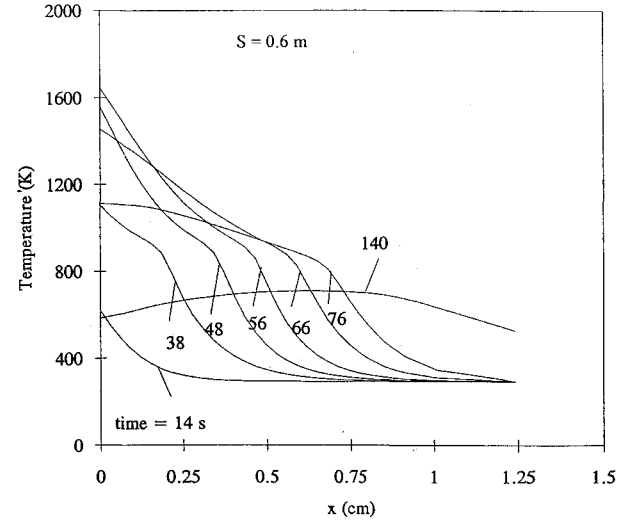

Fig. 5b In-depth temperature history.

those used in the LAURA code,[15] in which the collision integrals are evaluated as curve fits to tabular data.[16,17] The accuracy of transport properties for the $CO–CO_2$-dominated system is not well understood at present. The uncertainty in the wall catalysis model is one of the major limitations of heating accuracy.[18] The model for fully catalytic wall adopted in this study is from Ref. 19. The peak stagnation-point heating for the nonablating surface is about 112 W/cm^2, and for the ablating surface is about 85 W/cm^2. In the conical region, the minimum heating for the ablating surface is below 30 W/cm^2. Despite the small (normalized) mass blowing rate, which is only 0.7% of the freestream mass flow, the calculation indicates that a substantial amount of heat flux is blocked. The injected pyrolysis gas remains near the surface, and dilutes the CO and O concentrations at the surface. Consequently, the net surface recombination rate for the ablating surface is low compared with that for the nonablating surface. The higher the surface blowing, the lower the number density of CO and O near the surface; thus the surface catalytic effect on the heating becomes less important as the surface blowing rate increases.

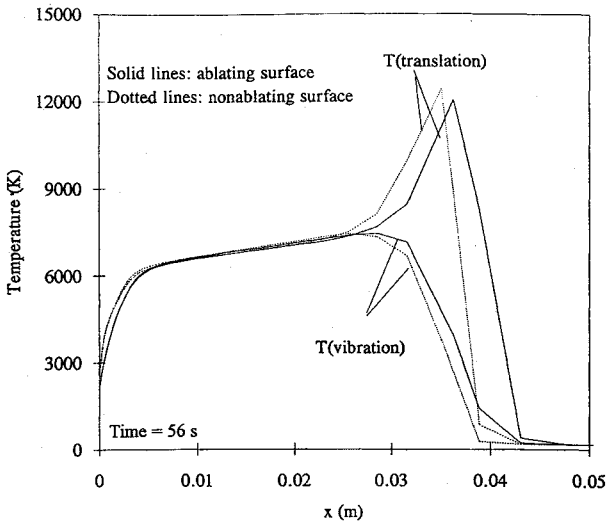

Fig. 6a Stagnation-streamline temperature profiles.

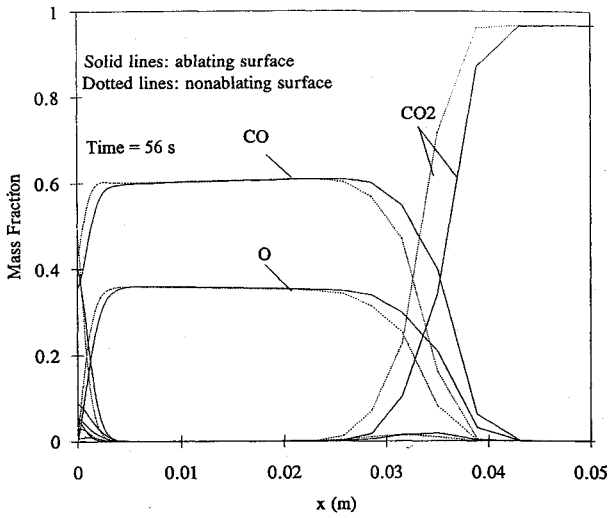

Fig. 6b Stagnation-streamline species concentration profiles.

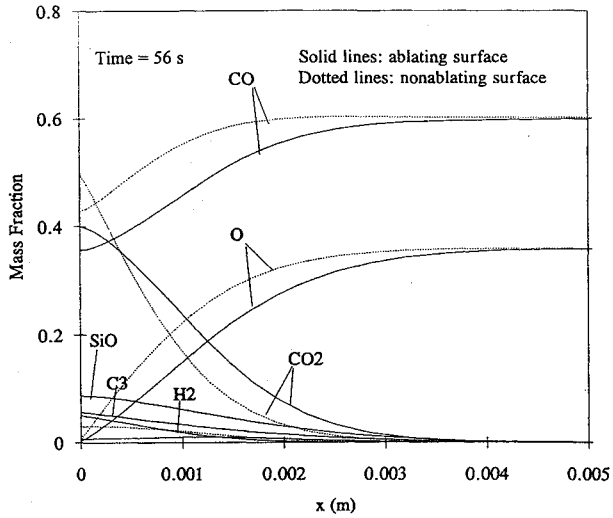

Fig. 6c Stagnation-streamline species concentration profiles.

Figures 3a and 3b show the histories of surface temperature, mass blowing rate, and heat flux at the stagnation point, and Figs. 4a and 4b show these same values at $S = 0.6$ m. The calculations predict that the peak mass blowing rate occurs at around $t = 35$ s for the stagnation point ($S = 0$) and at around $t = 40$ s for $S = 0.6$ m. Note that the surface blowing rate reaches its peak value before the surface heating and temperature. As the temperature increases, the decomposition rate is essentially an exponential function of local

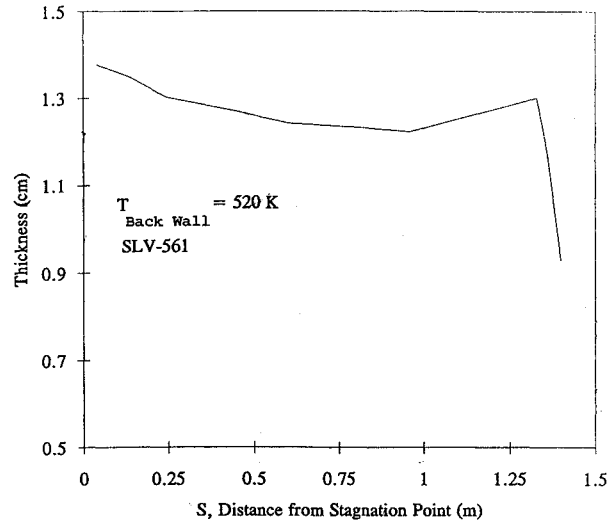

Fig. 7 Heat-shield thickness distribution.

material temperature [Eq. (4)]. However, as the density loss becomes significant, the density loss term offsets the temperature effect and gradually reduces the decomposition rate. The in-depth conduction and the radiative heating are about equally important and cannot be ignored over at least about one-third of the trajectory. The in-depth conduction becomes negative late in the trajectory. This is due to the dramatic reduction of surface heating, which causes the surface to become cooler than the in-depth char.

The in-depth temperature profiles ($t = 14$, 38, 48, 56, 66, 76, and 140 s) at the locations $S = 0$ and 0.6 m are presented in Figs. 5a and 5b, respectively. The trends of in-depth temperature histories for both locations are similar. A sharp change of temperature gradient appears in the temperature profiles for most trajectory times except the very early ($t = 14$ s) and late ($t = 140$ s) times, and the locations of these gradient changes gradually move deeper into the solid as the time increases. This effect results from the change of thermal conductivity as pyrolysis occurs. Therefore, slope change is an approximate marker for the bottom of the pyrolysis zone. Thus, from the in-depth temperature profiles, the total mass loss at certain locations can be roughly estimated. Since CMA is a one-dimensional code, the in-depth conduction for each surface station is assumed to be one-dimensional (normal to surface); that is, the thermal conduction transverse to the surface is ignored. This is a reasonable assumption over most of the aeroshell forebody except the shoulder, where the temperature gradient is high in the direction along the surface (see Fig. 2a).

The temperature distributions along the stagnation streamline at the peak convective heating point are shown in Fig. 6a, and the species concentration profiles are illustrated in Fig. 6b. The solutions for both ablating surface condition (solid lines) and nonablating surface condition (dotted lines) are presented. The surface blowing causes the shock standoff distance for the ablating surface to be slightly larger than that for the nonablating surface. Blowing also increases the boundary-layer thicknesses, as is to be expected. Figure 6c presents the species distributions in a region 0.5 cm next to the stagnation point, to depict more clearly the condition near the surface. Almost all the O atoms are consumed at the surface, but there are still some CO molecules left. This is because more CO than O is available at the surface and the surface is assumed to be fully catalytic for CO + O. For the ablating-surface calculation, the CO and O concentrations are lower than those for the nonablating-surface calculation. Thus, fewer CO and O are available at the surface for recombination reactions to occur. Consequently, less energy is released at the surface. The surface blowing reduces not only the thermal conduction to the surface but also the chemical energy from recombination at the surface (as a result of diffusion of CO and O to the surface).

Heat-shield thicknesses were computed and are presented in Fig. 7. In this calculation, the thicknesses were obtained in order to maintain the back-wall temperature at 520 K at 140 s, using the

conservative assumption that the back surface was adiabatic. The major limitation on the accuracy of the thickness calculation is the uncertainty in material properties, such as the thermal conductivity and enthalpy of pyrolysis gas. Using the material property database provided by Ref. 13, the computed thickness is 1.38 cm at the stagnation point, declines slightly in the conical region, and then increases at the junction between the cone and shoulder. The resulting heat-shield mass is about 20 kg. If the slightly conservative assumption is made, to facilitate manufacturing, that the thickness is uniformly 1.38 cm over the entire forebody, the mass becomes 21 kg. However, no factor of safety has been included.

Conclusion

A loosely coupled technique was developed to interface the GIANTS and CMA codes for two-dimensional axisymmetric and time-dependent trajectory-based heating analyses. The heat-shield (SLA-561V) thicknesses over Mars Pathfinder aeroshell forebody were obtained from the calculation. The solutions also include the detailed nonequilibrium flowfields, surface temperatures and heat fluxes, pyrolysis-gas blowing rates, and in-depth temperature history. The predictions indicate that surface blowing substantially reduces the heat flux to a surface. At the peak convective heating point, the stagnation-point heating for a nonablating fully catalytic surface is about 25% higher than for an ablating fully catalytic surface. Since the heat flux to a surface is very sensitive to surface catalysis as well as species diffusion rates, the development of more accurate transport-property models and surface catalysis models for CO_2 flow is required to improve the prediction of aerothermal heating. The present calculations yield a heat-shield mass, without a factor of safety, of about 20 kg.

Acknowledgment

Most of this task was performed under NASA Contract NAS2-14031 to Eloret.

References

[1]Hubbard, G. S., Wercinski, P. F., Sarver, G. L., Hanel, R. P., and Ramos, R., "A Mars Environmental Survey (MESUR)—Feasibility of a Low Cost Global Approach," International Astronautical Federation, IAF Paper 91-432, Oct. 1991.

[2]Anon., "Entry Data Analysis for Viking Landers," Martin Marietta Corp., Rept. TN-3770218, Denver, CO, Nov. 1976.

[3]Chen, Y.-K., "Effect of Non-Equilibrium Flow Chemistry on the Heating Distribution over the MESUR Forebody During a Martian Entry," NASA CR-177601, Sept. 1992.

[4]Chen, Y.-K., Henline, W. D., Stewart, D. A., and Candler, G. V., "Navier–Stokes Solutions with Surface Catalysis for Martian Atmospheric Entry," *Journal of Spacecraft and Rockets*, Vol. 30, No. 1, 1993, pp. 32–42.

[5]Tauber, M. E., Henline, W. D., Chargin, M., Papadopoulos, P., Chen, Y., Yang, L., and Hamm, K., "Mars Environmental Survey Probe Aerobrake Preliminary Design Study," *Journal of Spacecraft and Rockets*, Vol. 30, No. 4, 1993, pp. 431–437.

[6]Anon., *User's Manual: Aerotherm Charring Material Thermal Response and Ablation Program CMA87S*, Acurex UM-87-13/ATD, Acurex Corp., Nov. 1987.

[7]Chen, Y.-K., and Henline, W. D., "Analysis of Hypersonic Arcjet Flow Fields and Surface Heating of Blunt Bodies," AIAA Paper 93-0272, Jan. 1993.

[8]Chen, Y.-K., and Henline, W. D., "Chemical Nonequilibrium Navier–Stokes Solutions for Hypersonic Flow over an Ablating Graphite Nosetip," AIAA Paper 93-2836, July 1993.

[9]Tauber, M. E., and Sutton, K., "Stagnation-Point Radiative Heating Relations for Earth and Mars Entries," *Journal of Spacecraft and Rockets*, Vol. 28, No. 1, 1991, pp. 40–42.

[10]Park, C., Howe, J. T., Jaffe, R. L., and Candler, G. V., "Review of Chemical Kinetics Problems of Future NASA Missions, II: Mars Entries," *Journal of Thermophysics and Heat Transfer*, Vol. 8, No. 1, 1994, pp. 9–23.

[11]Bhutta, B. A., and Lewis, C. H., "A New Technique for Low-to-High Altitude Predictions of Ablative Hypersonic Flowfields," *Journal of Spacecraft and Rockets*, Vol. 29. No. 1, 1992, pp.35–50.

[12]Sangisvanni, J. J., and Barber, T. J., " Role of Hydrogen/Air Chemistry in Nozzle Performances for a Hypersonic Propulsion System," *Journal of Propulsion and Power*, Vol. 9, No. 1, 1993, pp. 178–183.

[13]Congdon, W. M., "Pathfinder Project SLA-561V Heat Shield—Thermophysical Test Data Base and Charring Ablation Response Model Parameters," Applied Research Assoc., Rept. ARA/93/5832/2, Dec. 1993.

[14]Mitcheltree, R. A., private communication, NASA Langley Research Center, Hampton, VA, Jan. 1994.

[15]Gnoffo, P. A., Gupta, R. N., and Shinn, J. L., "Conservation Equations and Physical Models for Hypersonic Air Flows in Thermal and Chemical Nonequilibrium," NASA TP-2867, Feb. 1989.

[16]Gupta, R. N., Yos, J. M., and Thompson, R. A., "A Review of Reaction Rates and Thermodynamic and Transport Properties for the 11-Species Air Model for Chemical and Thermal Nonequilibrium Calculations to 30000 K," NASA TM-101528, Feb. 1989.

[17]Mitcheltree, R. A., "Aerothermodynamics of a MESUR Martian Entry," AIAA Paper 93-2761, July 1993.

[18]Gupta, R. N., and Lee, K. P., "An Aerothermal Study of MESUR Pathfinder Aeroshell," AIAA Paper 94-2025, June 1994.

[19]Mitcheltree, R. A., and Gnoffo, P. A., "Wake Flow About a MESUR Mars Entry Vehicle," AIAA Paper 94-1958, June 1994.

K. J. Weilmuenster
Associate Editor